Nonlinear Response of Functionally Graded Panels with stiffeners in Supersonic Flow

(Received: September 24, 2016. Revised: October 26, 2016. Accepted: January 31, 2017)

M.R. Amoozgar[1]
H. Shahverdi[2]
H.R. Ovesy[3]

Abstract
This paper aims to study the nonlinear response of a stiffened functionally graded plate in supersonic flow. To model the geometrically nonlinear behavior of the stiffened panel, the von Karman large deflection plate theory is employed and the stiffener which is placed on the plate in different positions is modeled by using the Euler-Bernoulli beam theory. These two structural models are coupled to each other via a pair of action-reaction forces. The plate is in the supersonic regime and the quasi-steady first order piston theory is utilized to estimate the aerodynamic pressure induced by the supersonic flow. By using the Hamilton's principle the nonlinear partial differential equations of the stiffened panel are obtained. These partial differential equations are converted to ordinary differential equations by using the Galerkin's method which then solved by numerical integration. It is found that by using the stiffeners, the onset of flutter and also the limit cycle oscillation amplitude of the system changes dramatically and the rate of this change extremely depends on the volume fraction index of the plate made of functionally graded materials and the plate aspect ratio. Moreover, the effect of number of stiffeners on the aeroelastic behavior of FG panel is studied and it is clarified that by increasing the number of stiffeners, the flutter boundary increases.

1 Introduction

Panel flutter is a classical and important problem in the field of aeroelasticity which is studied by many researchers. When a surface of an aerial vehicle being subjected to supersonic flow it may start to oscillate. The value of the dynamic pressure in which the surface starts to oscillate is called the critical dynamic pressure. The value of critical dynamic pressure is determined by simple linear models while the post critical response of the system can only be examined by nonlinear theories. In this study, the nonlinear structural model is used for capturing the nonlinear post-instability of the panel.
The nonlinear response of supersonic panels in terms of limit cycle oscillation has been considered by many authors. Among all studies in this field, the first and the most important ones were the study of nonlinear oscillation of simply supported fluttering plates which was considered by Dowell [6, 7]. These works have been continued by considering the nonlinear flutter of doubly curved panels [8, 9]. The results confirmed that the stream-wise curvature has a destabilizing effect on the onset of instability. Weiliang and Dowell [24] investigated the limit cycle oscillation of a cantilever plate. They used a Rayleigh-Ritz approach and showed that the length to width ratio of the cantilever has a significant effect on the flutter instability of panels. All these studies were dedicated to isotropic materials while nowadays their usage has been limited and modern materials used more commonly.
One of the current methods used often to enhance the structural strength of

[1] Ph.D Student, Department of Aerospace Engineering and Center of Excellence in Computational Aerospace Engineering, Amirkabir University of Technology, Tehran, Iran
[2] Assistant Professor, Department of Aerospace Engineering and Center of Excellence in Computational Aerospace Engineering, Amirkabir University of Technology, Tehran, Iran
[3] Professor, Department of Aerospace Engineering and Center of Excellence in Computational Aerospace Engineering, Amirkabir University of Technology, Tehran, Iran

doi:10.3293/asdj.2017.41

aerial vehicles and also to keep their weight as low as it can be, is to use the composite materials. Thought composite materials have many advantages, they are suffering from some disadvantages. Therefore, in order to overcome these disadvantages, functionally graded materials (FGMs) was proposed [18]. The FGM materials are widely used in advanced air vehicle structures [16] and received more attentions in recent aeroelastic studies. The aeroelastic analysis of functionally graded panels has been considered by many researchers and a comprehensive review of the literature in this field is beyond the scope of this paper. Therefore, here only some important studies will be highlighted. The nonlinear transient thermoelastic analysis of functionally graded ceramic-metal plates was considered by Praveen and Reddy [20]. They showed that the plate's response is not the average of the response of the ceramic and the metal plates when the material properties are between those of ceramic and metal. Feldman and Aboudi [10] investigated the buckling of FGM plates subjected to uniaxial loading. They showed that the buckling load improved by using the functionally graded materials as compared to the corresponding uniformly reinforced plates. The effect of thermal stresses on the supersonic flutter behavior of functionally graded flat panels was investigated by Prakash and Ganapathi [19] by using the finite element procedure. They highlighted the influence of aerodynamic damping and thermal gradient on the flutter behavior of functionally graded plates. Haddadpour et al. [11] studied the nonlinear post flutter response of a functionally graded plate by using the Galerkin's method and showed by using FGM materials instead of pure metal materials, the instability margin of the plate is enhanced. Thermal flutter characteristics of functionally graded ceramic/metal panels under the thermal and aerodynamic loads were investigated by Sohn and Kim [22]. The results indicated that by increasing the volume fraction, the critical aerodynamic pressure increases and the limit cycle amplitude decreases. Navazi and Haddadpour [17] considered the parametric study of the nonlinear aero-thermoelastic behavior of functionally graded plates. They investigated the effects of different parameters on the nonlinear aeroelastic behavior of FG flat plates and highlighted that for in-plane loading of functionally graded plates with temperature-independent material properties, the Mori-Tanaka scheme may result to lower stability capacity than by the simple rule of mixture. Supersonic flutter of functionally graded open conical shell plates with clamped and simply supported edges has been considered by Davar and Shokrollahi [5]. They showed that the discrepancies between the results of the first order shear deformation and classical shell theories in determining the critical aerodynamic pressure are higher than for determining the frequencies. Shahverdi et al. [21] investigated the aero-thermo-elasticity of FG plates by using the generalized differential quadrature method. They showed that their proposed numerical solution has very accurate results in accordance with its low computational efforts.

The other way to enhance the strength of a structure without having weight penalty in engineering applications is to use the stiffeners instead of increasing the thickness of the whole structure. This way is very common in aerospace structures and the effects of adding stiffeners to the structural must be investigated in terms of structural stability and dynamics. There are some papers concerning this type of studies. Liao and Sun [15] investigated the flutter instability of stiffened and non-stiffened laminated composite plates and shells in supersonic flow by using the finite element method. It was concluded that the subtended angle, lamination scheme, skew angle, and number and position of the stiffeners affect the flutter instability of plates and shells. The effect of stiffener size and the fiber orientation angle on the flutter onset of the stiffened anisotropic laminated and isotropic panel was determined by Lee and Lee [13]. Lee at al. [14] studied the linear and nonlinear thermal flutter of a stiffened composite panel subjected to supersonic flow using FEM. They showed that the proper stiffening scheme can result in better flutter characteristics. The

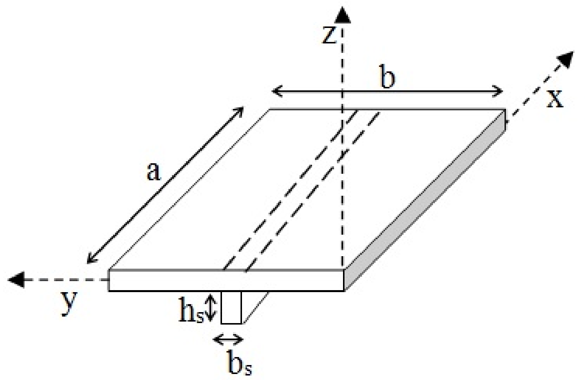

Figure 1: Stiffened panel geometry

aeroelastic behavior of stiffened laminated composite panels in supersonic flow has been considered by Zhao and Cao [25]. This study is important because of the method used for adding the effect of stiffeners to the governing equations. They developed a new analytical model to consider the effect of the stiffener on the plate behavior. This is done by considering a pair of acting and reacting forces. Vibration and dynamic stability of stiffened plates subjected to in-plane harmonic edge loading by FE method were studied by Srivastava et al. [23]. They highlighted that the instability margin of the system varies by considering or neglecting the in-plane displacement. Kaihua and Zhiping [12] investigated the nonlinear aeroelasticity of stiffened composite panels in supersonic aerodynamic flow. They used the finite element method along with Bogner-Fox-Schmit elements and determined that the stiffening scheme has significant effect on the flutter critical dynamic pressure.

In the present study, the aeroelastic stability and limit cycle oscillations of stiffened FG plates are investigated for the first time. In this regards, the system of panel and stiffener is modeled by using the von-Karman large deflection plate and the Euler-Bernoulli beam theory, respectively. These two models are coupled to each other by a pair of action-reaction forces and are considered to be subjected to the supersonic flow. Finally, a computer program which is used the Adams-Moulton's method to solve the nonlinear coupled ordinary differential equations, is developed to determine the effect of stiffeners on flutter onset and post flutter response of functionally graded panels.

2 Governing Equations

A functionally graded plate with a merged stiffener as shown in Fig. 1 with length a, width b and thickness h has been considered here. The plate is subjected to a supersonic flow along the x direction and is strengthen by one or more stiffeners which are placed on the backside of the plate, parallel to the airflow. It is of note that the stiffener, regardless of its shape, affects the panel by its area and moment of inertia and therefore in this study the shape of the stiffener is not a concern. The stiffener length, width, and height are denoted here as a, b_s and h_s, respectively.

In order to consider the effect of the stiffener on dynamical equations of the panel, the deformation compatibility between the panel and the stiffener is considered. As shown in Fig. 2, the panel and the stiffener coupled to each other by a pair of action-reaction forces denoted as f_1(x,t) and f_2(x,t) ([25]).

As it was stated before, the governing equations of the panel and the stiffener determined based on von Karman large deformation plate theory and the Euler-Bernoulli beam theory, respectively.

Based on the Kirchhoff hypothesis, the displacements (u, v, w) of the panel are given as:

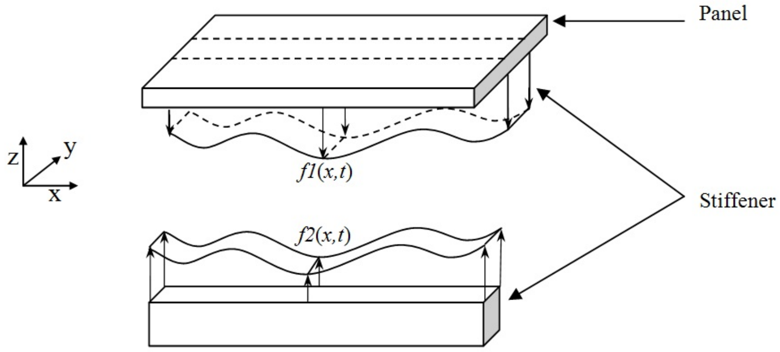

Figure 2: Schematic of the panel-stiffener action-reaction forces

$$
\begin{aligned}
u(x,y,z,t) &= u_0(x,y,t) - z\frac{\partial w_0(x,y,t)}{\partial x} \\
v(x,y,z,t) &= v_0(x,y,t) - z\frac{\partial w_0(x,y,t)}{\partial y} \\
w(x,y,z,t) &= w_0(x,y,t)
\end{aligned} \tag{1}
$$

where u_0, v_0 and w_0 are the middle surface displacement components along the x, y and z directions, respectively.
The nonlinear von Karman's strain-displacement expression for the panel are:

$$
\begin{aligned}
\epsilon_{xx} &= \frac{\partial u_0}{\partial x} + \frac{1}{2}(\frac{\partial w_0}{\partial x})^2 - z\frac{\partial^2 w_0}{\partial x^2} \\
\epsilon_{yy} &= \frac{\partial v_0}{\partial y} + \frac{1}{2}(\frac{\partial w_0}{\partial y})^2 - z\frac{\partial^2 w_0}{\partial y^2} \\
\epsilon_{xy} &= \frac{1}{2}(\frac{\partial u_0}{\partial y} + \frac{\partial v_0}{\partial x} + \frac{\partial w_0}{\partial y}\frac{\partial w_0}{\partial x}) - z\frac{\partial^2 w_0}{\partial x \partial y}
\end{aligned} \tag{2}
$$

The stress-strain relations are expressed by the Hooke's law as:

$$
\begin{Bmatrix} \sigma_{xx} \\ \sigma_{yy} \\ \sigma_{xy} \end{Bmatrix} = \begin{Bmatrix} Q_{11} & Q_{12} & 0 \\ Q_{12} & Q_{22} & 0 \\ 0 & 0 & Q_{66} \end{Bmatrix} \begin{Bmatrix} \epsilon_{xx} \\ \epsilon_{yy} \\ 2\epsilon_{xy} \end{Bmatrix} \tag{3}
$$

where, the stiffness coefficients, Q_{ij} , are:

$$
\begin{aligned}
Q_{11} = Q_{22} &= \frac{E(z)}{1-\nu(z)^2} \\
Q_{12} &= \frac{\nu(z)E(z)}{1-\nu(z)^2} \\
Q_{66} &= \frac{E(z)}{2[1+\nu(z)]}
\end{aligned} \tag{4}
$$

and E(z) and (z) are Young's modulus and Poisson's ratio of the FG panel defined as follow ([4]):

$$
\begin{aligned}
E(z) &= (E_C - E_M)(\frac{2z+h}{2h})^n + E_M \\
\nu(z) &= (\nu_C - \nu_M)(\frac{2z+h}{2h})^n + \nu_M
\end{aligned} \tag{5}
$$

where, n is the volume fraction exponent and subscripts C and M refer to the ceramic and the metal properties of the FG panel, respectively.

The equations of motion are derived using Hamilton's principle:

$$\int_0^T (\delta K - \delta U + \delta V)dt = 0 \tag{6}$$

where δU, the virtual strain energy, δV, the virtual work done by aerodynamic forces and stiffener action and δK, the virtual kinetic energy, are given by ([25]):

$$\begin{aligned}
\delta U &= \int_{A_0}\int_{-h/2}^{h/2} (\sigma_{xx}\delta\epsilon_{xx} + \sigma_{yy}\delta\epsilon_{yy} + 2\sigma_{xy}\delta\epsilon_{xy})dzdxdy \\
\delta V &= \int_{A_0} [f_1(x,t)\tilde{\delta}(y-\xi)b_s\delta W(x,\xi,-h/2) - \Delta p\delta W(x,y,h/2)]dxdy \\
\delta K &= \int_{A_0}\int_{-h/2}^{h/2} \rho(z)[(\dot{u_0} - z\frac{\partial \dot{w}_0}{\partial x})(\delta\dot{u_0} - z\frac{\partial \delta\dot{w}_0}{\partial x}) + \\
&\quad (\dot{v_0} - z\frac{\partial \dot{w}_0}{\partial y})(\delta\dot{v_0} - z\frac{\partial \delta\dot{w}_0}{\partial y}) + \dot{w}_0\delta\dot{w}_0]dzdxdy
\end{aligned} \tag{7}$$

where in these equations the Dirac delta function ($\tilde{\delta}$) and ξ are used in order to precisely consider the location and properties of the stiffener, A_0 is the plate area and $\rho(z)$ is the density of the FG panel ([4]):

$$\rho(z) = (\rho_C - \rho_M)(\frac{2z+h}{2h})^n + \rho_M \tag{8}$$

Also, f_1(x,t) is the acting force induced by transverse vibration of the stiffener, and may be defined as the Euler-Bernoulli beam vibrational equation ([25]):

$$\begin{aligned}
&f_1(x,t) = -f_2(x,t) \\
&E_sI_s\frac{\partial^4 w_s(x,t)}{\partial x^4} + \rho_s A_s\frac{\partial^2 w_s(x,t)}{\partial t^2} = f_2(x,t)
\end{aligned} \tag{9}$$

where E_s, I_s, ρ_s and A_s are Young's modulus, the mass moment of inertia, density and cross section area of the stiffener, respectively. The transverse displacement of the neutral axis of the stiffener is denoted here by w_s . By considering the deformation compatibility which was mentioned earlier, the stiffener mid-surface displacement will be:

$$w(x,y,t)|_{y=\xi} = w_s + \frac{h_s}{2}(1-\cos(\alpha)) \tag{10}$$

where α is the rotational displacement of the stiffener and based on the assumption that the displacement of the mid-plane of the stiffener in the z direction is small compared to its thickness approximately is equal to zero ([25]).
On the other hand, the aerodynamic pressure loading based on the quasi-steady first order supersonic piston theory is ([3]):

$$\Delta p = \frac{2q}{\beta}[\frac{\partial w(x,y,z)}{\partial x} + (\frac{M^2-2}{M^2-1})\frac{1}{V_\infty}\frac{\partial w(x,y,z)}{\partial t}] \tag{11}$$

where

$$\beta = \sqrt{M^2-1} \tag{12}$$

and

$$q = \frac{1}{2}\rho_a V_\infty^2 \tag{13}$$

and ρ^a is the density of air and V_∞ is the air speed.
By substituting Eqs. 2 and 3 into Eq. 7 and transferring the results into Eq. 6, the variation form of the Hamilto-nian in terms of displacement variations can be derived. By setting the coefficients of the virtual displacements δu_0, δv_0

and δw_0, to zero, the governing equations of motion can be obtained in terms of displacements for three-dimensional FGM plates as follow:

$$\begin{aligned}&A_{11}(\frac{\partial^2 u_0}{\partial x^2}+\frac{\partial w_0}{\partial x}\frac{\partial^2 w_0}{\partial x^2})+A_{12}(\frac{\partial^2 v_0}{\partial x\partial y}+\frac{\partial w_0}{\partial y}\frac{\partial^2 w_0}{\partial x\partial y})-B_{11}(\frac{\partial^3 w_0}{\partial x^3})\\&-B_{12}(\frac{\partial^3 w_0}{\partial x\partial y^2})+A_{66}(\frac{\partial^2 u_0}{\partial y^2}+\frac{\partial^2 v_0}{\partial x\partial y}+\frac{\partial w_0}{\partial y}\frac{\partial^2 w_0}{\partial x\partial y}+\frac{\partial w_0}{\partial x}\frac{\partial^2 w_0}{\partial y^2})\\&-2B_{66}(\frac{\partial^3 w_0}{\partial x\partial y^2})=I_0\ddot{u}_0-I_1\frac{\partial \ddot{w}_0}{\partial x}\end{aligned} \tag{14}$$

$$\begin{aligned}&A_{66}(\frac{\partial^2 u_0}{\partial x\partial y}+\frac{\partial^2 v_0}{\partial x^2}+\frac{\partial^2 w_0}{\partial x^2}\frac{\partial w_0}{\partial y}+\frac{\partial w_0}{\partial x}\frac{\partial^2 w_0}{\partial x\partial y})+A_{12}(\frac{\partial^2 u_0}{\partial x\partial y}+\frac{\partial w_0}{\partial x}\frac{\partial^2 w_0}{\partial x\partial y})\\&-2B_{66}(\frac{\partial^3 w_0}{\partial x^2\partial y})+A_{22}(\frac{\partial^2 v_0}{\partial y^2}+\frac{\partial w_0}{\partial y}\frac{\partial^2 w_0}{\partial y^2})-B_{12}(\frac{\partial^3 w_0}{\partial x^2\partial y})-B_{22}\frac{\partial^3 w_0}{\partial y^3}\\&=I_0\ddot{v}_0-I_1\frac{\partial \ddot{w}_0}{\partial y}\end{aligned} \tag{15}$$

$$\begin{aligned}&B_{11}(\frac{\partial^3 u_0}{\partial x^3}+\frac{\partial^2 w_0}{\partial x^2}\frac{\partial^2 w_0}{\partial x^2}+\frac{\partial w_0}{\partial x}\frac{\partial^3 w_0}{\partial x^3})+B_{12}(\frac{\partial^3 v_0}{\partial x^2\partial y}+\frac{\partial^2 w_0}{\partial x\partial y}\frac{\partial^2 w_0}{\partial x\partial y}\\&+\frac{\partial w_0}{\partial x}\frac{\partial^3 w_0}{\partial x^2\partial y})-D_{11}(\frac{\partial^4 w_0}{\partial x^4})-2D_{12}(\frac{\partial^4 w_0}{\partial x^2\partial y^2})-4D_{66}(\frac{\partial^4 w_0}{\partial x^2\partial y^2})\\&-D_{22}(\frac{\partial^4 w_0}{\partial y^4})+2B_{66}(\frac{\partial^3 u_0}{\partial x\partial y^2}+\frac{\partial^3 v_0}{\partial x^2\partial y}+\frac{\partial^3 w_0}{\partial x^2\partial y}\frac{\partial w_0}{\partial y}+\frac{\partial^2 w_0}{\partial x\partial y}\frac{\partial^2 w_0}{\partial x\partial y}\\&\frac{\partial^2 w_0}{\partial x^2}\frac{\partial^2 w_0}{\partial y^2}+\frac{\partial w_0}{\partial x}\frac{\partial^3 w_0}{\partial x\partial y^2})+B_{12}(\frac{\partial^3 u_0}{\partial x\partial y^2}+\frac{\partial^2 w_0}{\partial x\partial y}\frac{\partial^2 w_0}{\partial x\partial y}+\frac{\partial w_0}{\partial x}\frac{\partial^3 w_0}{\partial x\partial y^2})\\&+B_{22}(\frac{\partial^3 v_0}{\partial y^3}+\frac{\partial^2 w_0}{\partial y^2}\frac{\partial^2 w_0}{\partial y^2}+\frac{\partial w_0}{\partial y}\frac{\partial^3 w_0}{\partial y^3})+\bar{N}(w_0)\\&-\frac{2q}{\beta}[\frac{\partial w_0}{\partial x}+(\frac{M^2-2}{M^2-1})\frac{1}{V_\infty}\dot{w}_0]+f_1(x,t)\tilde{\delta}(y-\xi)b_s\\&I_0\ddot{w}_0-I_2(\frac{\partial^2 \ddot{w}_0}{\partial x^2}+\frac{\partial^2 \ddot{w}_0}{\partial y^2})+I_1(\frac{\partial \ddot{u}_0}{\partial x}+\frac{\partial \ddot{v}_0}{\partial y})\end{aligned} \tag{16}$$

where A_{ij} ,B_{ij} and D_{ij} are the extensional stiffness, the bending-extensional coupling stiffness , bending stiffness and mass moment of inertias and may be expressed as:

$$\begin{aligned}(A_{ij},B_{ij},D_{ij})&=\int_{-h/2}^{h/2}Q_{ij}(1,z,z^2)dz; i,j=1,2,6\\(I_0,I_1,I_2)&=\int_{-h/2}^{h/2}\rho(z)(1,z,z^2)dz\end{aligned} \tag{17}$$

and the nonlinear in-plane load operator appeared in Eq. 15, $\bar{N}(w_0)$, is ([1]):

$$\bar{N}(w_0)=\frac{\partial}{\partial x}(N_{xx}\frac{\partial w_0}{\partial x}+N_{xy}\frac{\partial w_0}{\partial y})+\frac{\partial}{\partial y}(N_{xy}\frac{\partial w_0}{\partial x}+N_{yy}\frac{\partial w_0}{\partial y}) \tag{18}$$

where N_{xx}, N_{xy} and N_{yy} are the force resultants determined.

3 Solution Methodology

The boundary conditions of the plate is assumed to be simply supported along all edges with the following conditions:

	Young's modulus (Gpa)	Density (kg/m3)	Poisson's ration
Aluminum	70	2700	0.3
Zirconia	151	3000	0.3

Table 1: Material properties of Aluminum and Zirconia

$$\begin{aligned} u_0 = v_0 = w_0, \quad & M_x = 0 \quad at \quad x = 0, a \\ u_0 = v_0 = w_0, \quad & M_y = 0 \quad at \quad y = 0, b \end{aligned} \tag{19}$$

The trial functions that satisfy these boundary conditions can be written as:

$$\begin{aligned} u_0(x, y, t) &= \sum_{i=1}^{\infty} \sum_{m=1}^{\infty} a_{im}(t) \sin(\frac{i\pi x}{a}) \sin(\frac{m\pi y}{b}) \\ v_0(x, y, t) &= \sum_{j=1}^{\infty} \sum_{m=1}^{\infty} b_{jm}(t) \sin(\frac{j\pi x}{a}) \sin(\frac{m\pi y}{b}) \\ w_0(x, y, t) &= \sum_{k=1}^{\infty} \sum_{m=1}^{\infty} c_{km}(t) \sin(\frac{k\pi x}{a}) \sin(\frac{m\pi y}{b}) \end{aligned} \tag{20}$$

where i and m are the number of modes in the x and y directions, respectively. Based on the literature, in this study four stream-wise (x direction) modes and one span-wise (y direction) mode are retained ([7]) for the aeroelastic analysis. By substituting the modes assumed in Eq. 20 into the Eqs. 14-16, and then applying Galerkin's procedure and multiplying each part of these equations by the same mode shape and integrating over the panel area, one obtains a set of nonlinear ordinary differential equations in the time domain that in compact form can be written as follow:

$$\mathbf{M}\ddot{\mathbf{q}} + \mathbf{C}\dot{\mathbf{q}} + \mathbf{K}(\mathbf{q})\mathbf{q} = 0 \tag{21}$$

where $\mathbf{q}$ is the vector of unknown parameters, $\mathbf{M}$, $\mathbf{C}$ and $\mathbf{K}$ are the resultant mass matrix, damping matrix and stiffness matrix, respectively.
Let consider a vector as:

$$y = [a_{11}, \dot{a_{11}}, b_{11}, \dot{b_{11}}, c_{11}, \dot{c_{11}}, ..., a_{i1}, \dot{a_{i1}}, b_{i1}, \dot{b_{i1}}, c_{i1}, \dot{c_{i1}}] \tag{22}$$

then Eq. 21, can be written in the following form:

$$\dot{y} = \mathbf{A}y + f(y) \tag{23}$$

This first order nonlinear ODE can be solved by numerical integration method. In this study, the Adams-Moulton's method has been used to integrate the nonlinear differential equations.

4 Numerical Results

The FGM panel is made of Aluminum and Zirconia with the material properties listed in Table 1, and the stiffener is considered to be made of Aluminum.

Due to numerical usefulness, the results will be presented in non-dimensional form. The non-dimensional para-meters used throughout the paper are:

$$\xi = x/a, \eta = y/b, \lambda = \frac{2qa^3}{\beta D_{11M}}, h^* = h_s/h, b^* = b_s/b$$

To check the accuracy of the proposed model and also verifying the developed program, the post flutter time responses of FGM plates are determined and the limit cycle amplitudes are compared with the results of Haddadpour et al. [11] for an infinitely long plate in Fig. 3. As it can be seen, a good agreement

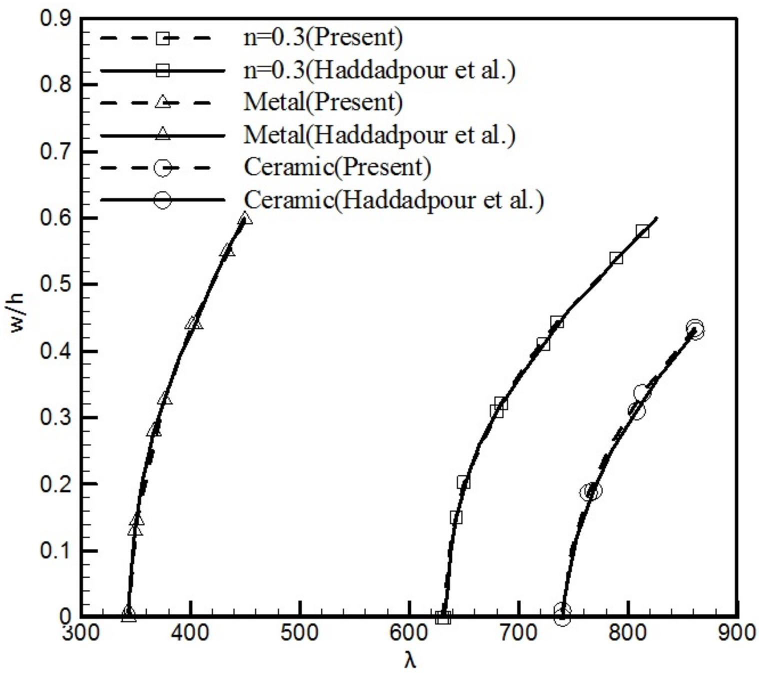

Figure 3: Non-dimensional limit cycle amplitude versus non-dimensional dynamic pressure parameter, λ

Table 2: Comparison of the natural frequencies of the stiffened panel (Hz) with $h = 6.33e-3m, l = 0.41m, b = 0.6m, h_s = 22.22e-3m, b_s = 12.7e-3m, E = 2.11e11N/m^2, \rho = 7.83e3Kg/m^3, \nu = 0.3$

Mode	Aksu [2]	present	Err. %
1	254.94	255.59	0.25
2	269.46	266.47	-1.1
3	511.64	502.6	-1.7

between the results is observed.

On the other hand, to check the validity of the structural dynamic characteristics of the panel with stiffener, the three first natural frequencies of the stiffened panel are compared with the results presented by Aksu [2] and reported in Table 2. It is noted that the natural frequencies of the stiffened panel are calculated by determining the eigenvalues of the linearized system of Eq. 21 about the equilibrium point y=0. It is obvious from this table that the dynamic characteristics of the developed model are in good agreement with those obtained in [2]. Small differences come from the fact that in the present study the effect of in-plane inertia, torsional stiffness, and warping of the cross section of the stiffener are neglected. It is worth mentioning that in this part of the paper to capture the second and third natural frequencies of the stiffened panel, four span-wise (y direction) and four stream-wise (x direction) modes are retained in the Galerkin's procedure.

In order to check the convergence of the developed code for different number of stream-wise modes, the instability onset dynamic pressure for different values of m has been calculated and reported in Table 3. Here the panel is considered to be square with one centrally spaced stiffener, and the width and the thickness of the stiffener are $b^* = 0.02$ and $h^* = 10$, respectively. As it is clear here, for a stiffened panel by considering four stream-wise modes, the results were generally converged within 1% error.

Fig. 4 shows the non-dimensional limit cycle amplitude versus non-dimensional dynamic pressure, for various plate aspect ratios, (a/b), for volume fraction exponents $n = 5$. By increasing the plate aspect ratio, the critical dynamic pressure increases and a small increase in the aerodynamic pressure results in a

m	λ_{cr}
2	782.08
3	1058.92
4	1002.4
5	1015.65
6	1012.6
8	1012.27
10	1012.31

Table 3: Galerkin approach results for different mode numbers of a stiffened panel ($b^* = 0.02, h^* = 10$)

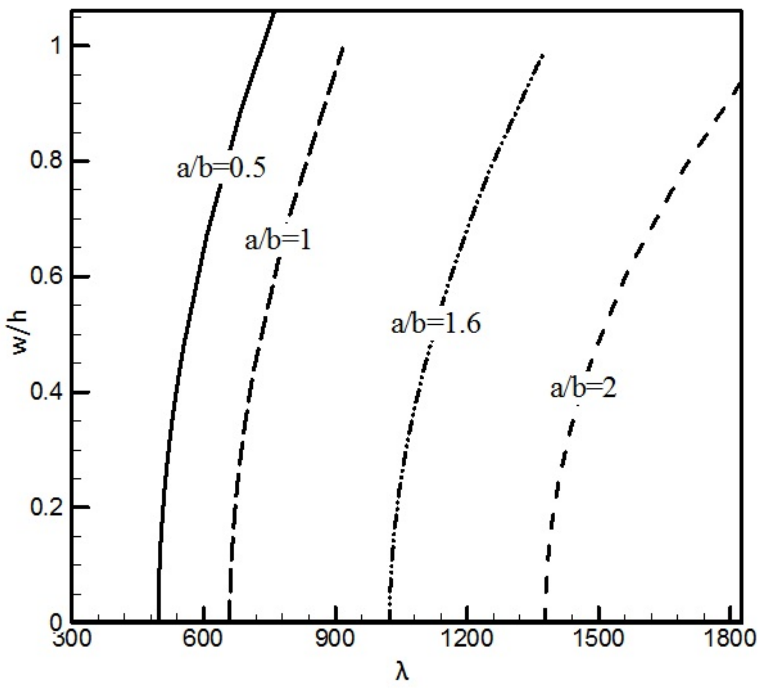

Figure 4: Non-dimensional limit cycle amplitude versus non-dimensional dynamic pressure parameter, λ, for n=5 and various plate aspect ratios, a/b

noticeable increase in the limit cycle amplitude.

Unless otherwise noted, the forthcoming results are related to a square stiffened panel ($a/b = 1$), and the LCO amplitudes correspond to the point $(0.75a, 0.5b)$ which is the critical point of oscillation.

Fig. 5 demonstrates the LCO amplitude of a FGM plate without stiffener for various volume fraction exponents. This plot will be considered as a base for comparison with following figures depicted to show the effects of adding stiffeners on the dynamic behavior of the system.

In the following sections, the effect of different parameters such as stiffener width, stiffener thickness, and number of stiffeners on both critical dynamic pressure and limit cycle amplitude of the stiffened panels with different aspect ratios are presented. The effect of the non-dimensional stiffener height on the limit cycle amplitude and the critical dynamic pressure of the panel are shown in Figs. 6 and 7 for various volume fraction exponents, respectively. The amplitude of the limit cycle oscillation is diminished by increasing the stiffener height. But in a certain range of the stiffener height, this reduction in the amplitude is more pronounced. The same trend is experienced among all volume fraction exponents. On the other hand, it is seen that the volume fraction exponent plays a decisive role in shifting the critical stiffener height at which a drastic drop in the amplitude is experienced. Fig. 7 demonstrates the critical dynamic pressure of the stiffened FG panel versus non-dimensional height of the stiffener for various volume fraction exponents. It is deduced that by increasing the stiffener height, the critical dynamic pressure of the panel increases for all volume fraction exponents. It is noted that in a certain region of the stiffener height, the dynamic pressure increases very rapidly and this region strongly depends

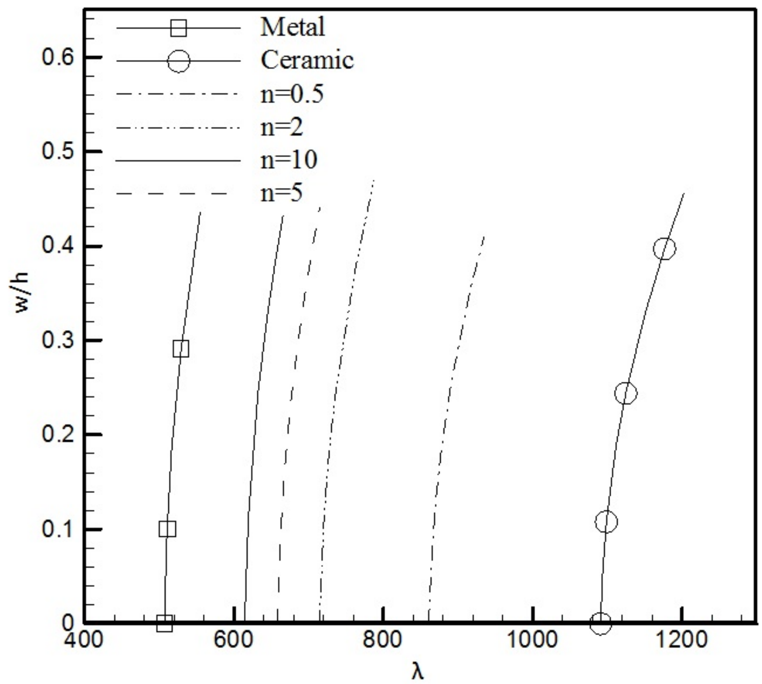

Figure 5: Non-dimensional limit cycle amplitude versus non-dimensional dynamic press parameter, λ, for various volume fraction exponents

on the values of volume fraction exponent, n.

The effect of the non-dimensional stiffener width on the non-dimensional limit cycle amplitude, and the critical dynamic pressure of the stiffened panel are shown in Figs. 8 and 9, respectively. As it is clear, by increasing the stiffener width, the LCO amplitude of the panel decreases for all fraction exponents. Therefore by widening the stiffener cross-section, the nonlinear aeroelastic post instability response of the panel can be improved. Fig. 9 describes the change of critical flutter dynamic pressure of the panel with respect to the variation of the stiffener width for various volume fraction exponents. The critical dynamic pressure of the panel enhances by increasing the width of the stiffener.

The effects of stiffener height and width on the critical dynamic pressure of FG panels for various aspect ratios are investigated, and reported in Figs 10 and 11, respectively. The volume fraction exponent of the FGM panel is assumed to be $n = 5$. Fig. 10 demonstrates the variation of critical dynamic pressure with respect to the stiffener height for four different aspect ratios, and Fig. 11 shows the variation of critical dynamic pressure of the panel for different stiffener width values. As it can be seen, the increase in the aspect ratio results in an increase in the critical dynamic pressure. Moreover, for higher aspect ratios, the variation of critical dynamic pressure with respect to the stiffener height, and width is more pronounced, when compared to the same variation but for the lower aspect ratios.

In Fig. 13, the limit cycle amplitude of the panel for various numbers of stiffeners has been depicted. It is clear that by increasing the number of stiffeners, the non-dimensional limit cycle amplitude of the panel changes. Moreover, the critical dynamic pressure of the panel increases by increasing the number of stiffeners. It must be noted that here the stiffeners are located in equal lengths along the y direction as shown in Fig. 12.

The effect of stiffener height on limit cycle amplitude of the FG panel for different number of stiffeners is shown in Fig. 14. By increasing the stiffener's height, the non-dimensional limit cycle amplitude decreases and the rate of this reduction strictly depends on the number of stiffeners. It is noted that for small values of stiffener height, the number of stiffeners does not have a significant effect on the LCO amplitude while for larger values, the number of stiffeners affects the amplitude dramatically.

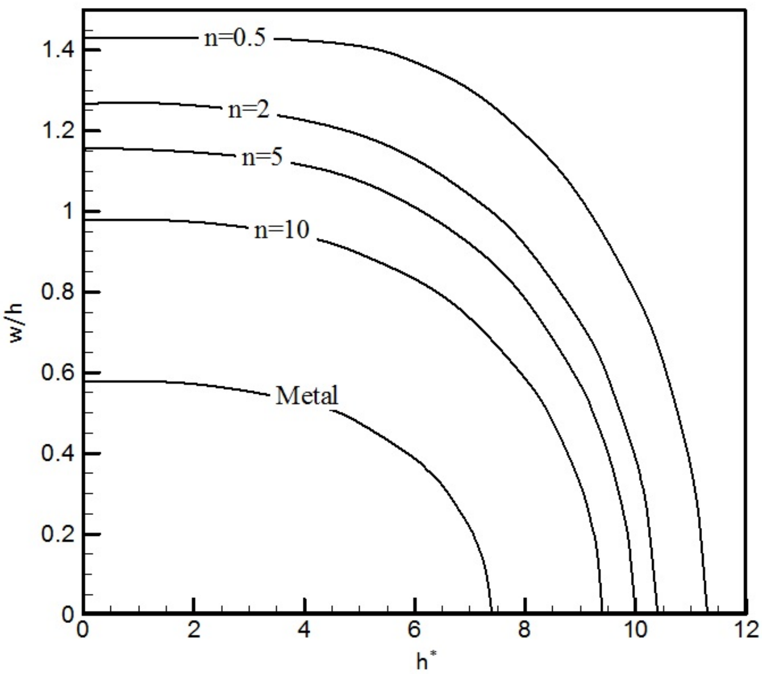

Figure 6: Effect of stiffener height on non-dimensional limit cycle amplitude for various volume fraction exponent and for $\lambda = 1000, b^* = 0.02$

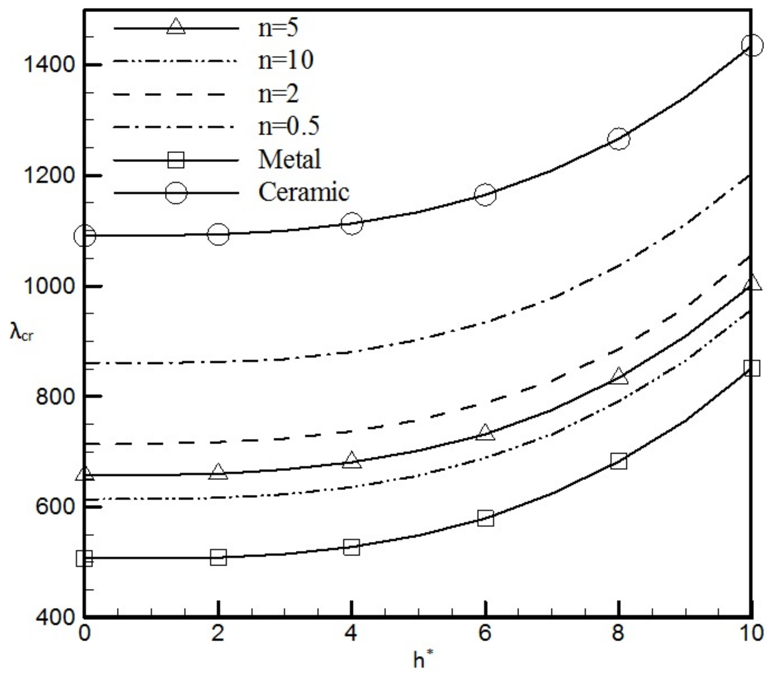

Figure 7: Effect of stiffener height on critical dynamic pressure for $b^* = 0.02$

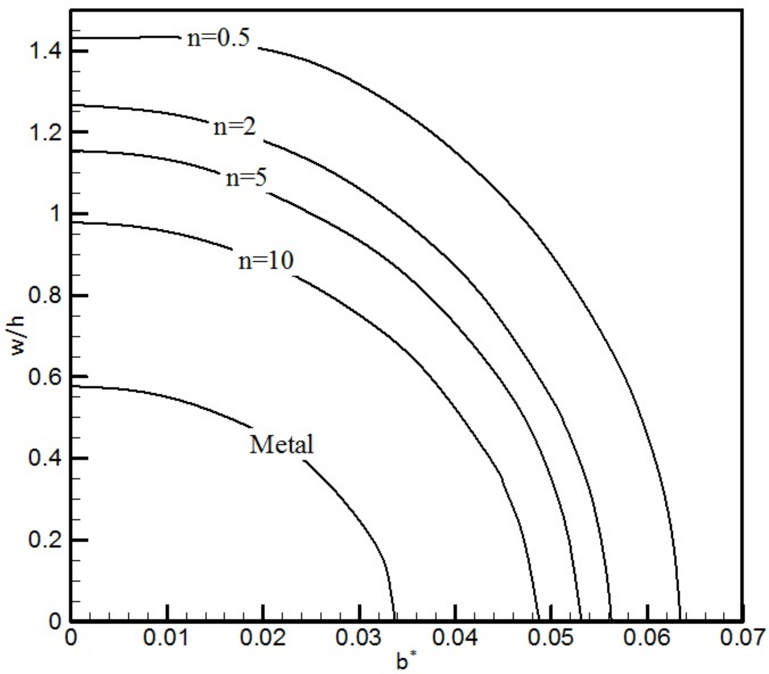

Figure 8: Effect of stiffener width on limit cycle amplitude for various volume fraction exponents and for $\lambda = 1000, h^* = 5$

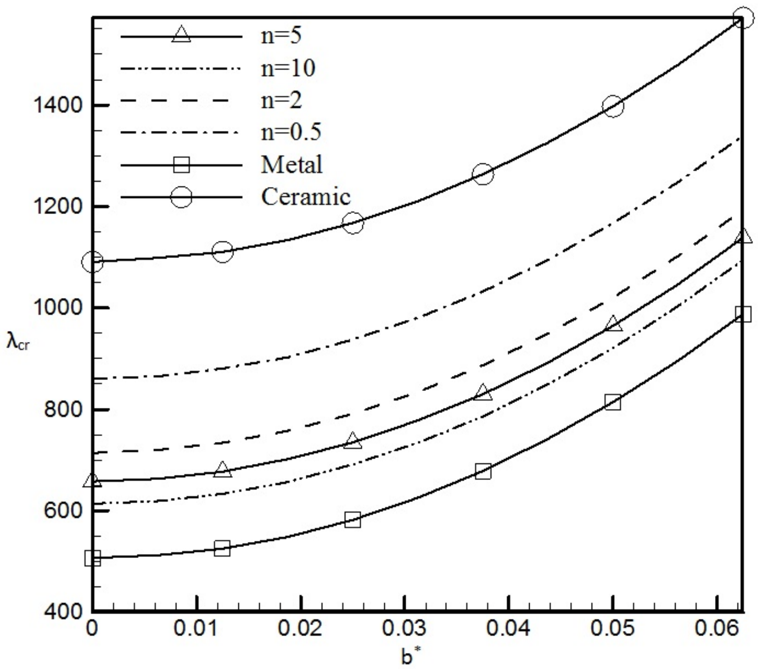

Figure 9: Effect of stiffener width on critical dynamic pressure for $h^* = 5$

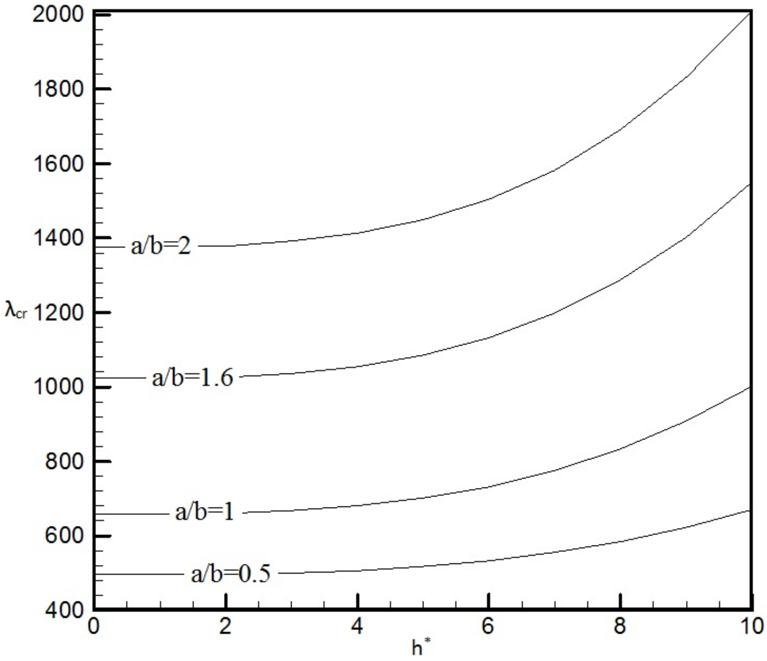

Figure 10: Effect of stiffener height on critical dynamic pressure for various aspect ratios when $b^* = 0.02, n = 5$

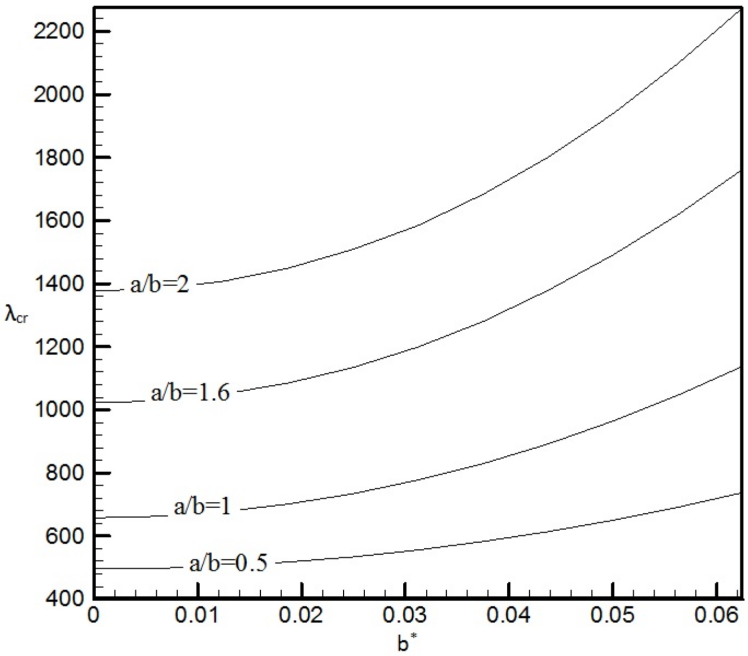

Figure 11: Effect of stiffener width on critical dynamic pressure for various aspect ratios when $h^* = 5, n = 5$

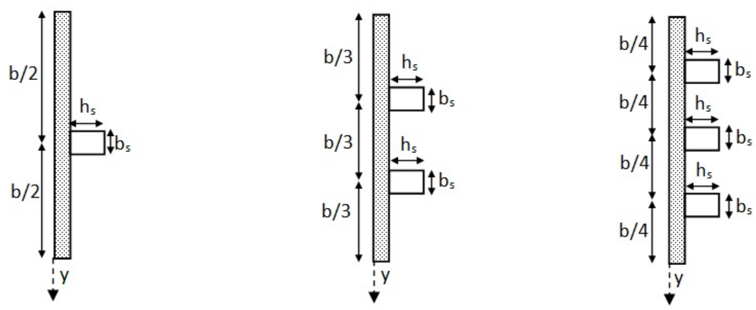

Figure 12: schematic of the stiffeners position

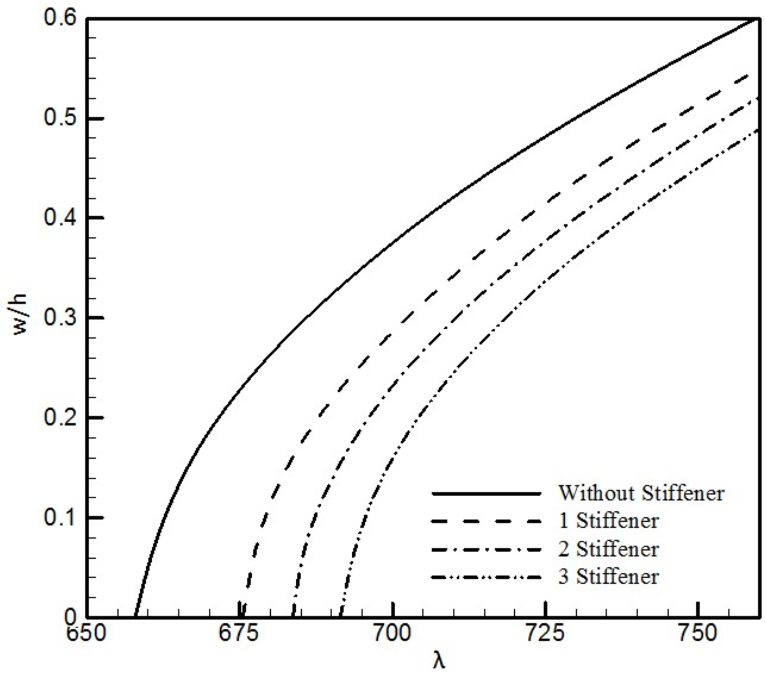

Figure 13: limit cycle amplitude of the FG panel for various numbers of stiffeners when $b^* = 0.025, h^* = 3, n = 5$

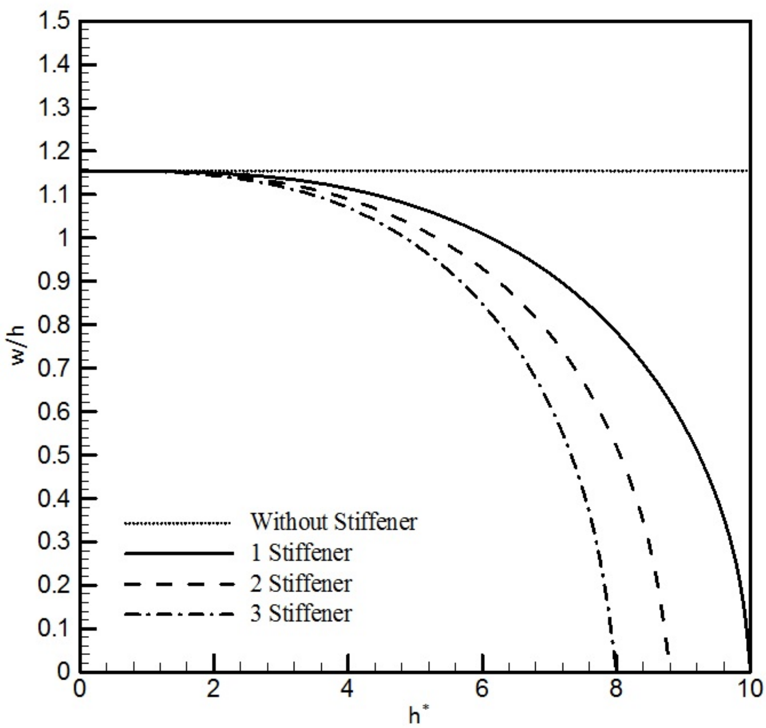

Figure 14: Effect of stiffener thickness and number of stiffeners on non-dimensional limit cycle amplitude for $\lambda = 1000, b^* = 0.025$

5 Conclusion

The nonlinear limit cycle oscillation of functionally graded stiffened plates was studied in supersonic flow regime. The von Karman large deflection plate theory along with the Euler-Bernoulli beam theory and the piston theory were employed to establish the governing aeroelastic equations of a stiffened panel. The resultant aero-elastic equations were solved by using the Galerkin's method and a numerical time marching method. By consi-dering all effective parameters of the system, the following points can be concluded:
The introduction of a stiffener into the FG panel affects both the limit cycle amplitude and the flutter margin of the FG panel, and the stiffener is much more effective for plates with higher aspect ratios and lower volume fraction exponents.
The height and the width of the stiffener have significant effects on the limit cycle amplitude of the FGM panel for all volume fraction exponents. However, the rate of variation of the critical dynamic pressure is dramatically dependent on the volume fraction exponents, stiffener number, height, and width and by increasing the number, height, and width of stiffeners, the critical dynamic pressure increases.
The optimum height and width of the stiffener to obviate the flutter onset of the FG panel is strongly depends on the volume fraction exponent, and therefore for an accurate instability investigation of the stiffened FG panels, all these parameters (stiffener dimensions, number, and volume fraction exponent) must be taken into account simultaneously.

References

[1] *Mechanics of laminated composite plates and shells*. 2nd edition Boca Raton (FL), CRC Press, 2004.

[2] G. Aksu. Free vibration analysis of stiffened plates by including the effect of in-plane inertia. *Journal of Applied Mechanics*, 49:206 – 212, 1982.

[3] H. Ashley and G. Zartarian. Piston theory- new aerodynamic toll for aeroelastician. *Journal of Aeronautical Sciences*, 23:1109 – 1118, 1956.

[4] K.Y. Dai, G.R. Liu, X. Han, and K.M. Lim. Thermomechanical analysis of functionally graded material (fgm) plates using element-free galerkin method. *Computers - Structures*, 83:1487 – 1502, 2005. Advances in Meshfree Methods.

[5] A. Davar and H. Shokrollahi. Flutter of functionally grade open conical shell panels subjected to supersonic air flow. *Proceeding of the Institude of Mechanical Engineering -Part G*, 27:1036 – 1052, 2013.

[6] EH. Dowell. Nonlinear oscillations of a fluttering plate. *AIAA Journal*, 4:1267 – 1275, 1966.

[7] EH. Dowell. Nonlinear oscillations of a fluttering plate ii. *AIAA Journal*, 5:1856 – 1862, 1967.

[8] EH. Dowell. Nonlinear flutter of curved plates. *AIAA Journal*, 7:424 – 431, 1969.

[9] EH. Dowell. Nonlinear flutter of curved plates ii. *AIAA Journal*, 8:259 – 261, 1970.

[10] E. Feldman and J. Aboudi. Analysis of functionally graded plates subjected to uniaxial loading. *Composite Structures*, 38:29 – 36, 1997.

[11] H. Haddadpour, H.M. Navazi, and F. Shadmehri. Nonlinear oscillations of a fluttering functionally graded plate. *Composite Structures*, 79:242 – 250, 2007.

[12] Y. Kaihua and Q. Zhiping. Nonlinear flutter analysis of stiffened composite panels in supersonic flow. *Science China Physics and Mechanics and Astronomy*, 53:336 – 344, 2010.

[13] DM. Lee and I. Lee. Supersonic flutter analysis of stiffened isotropic and anisotropic panels. *AIAA Journal*, 34:637 – 639, 1996.

[14] I. Lee, DM. Lee, and IK. Oh. Supersonic flutter analysis of stiffened laminated plates subjected to thermal load. *Journal of Sound and Vibration*, 244:49 – 67, 1999.

[15] CL. Liao and YW. Sun. Flutter analysis of stiffened laminated composite plates and shells in supersonic flow. *AIAA Journal*, 31:154 – 162, 1993.

[16] C. Mei and K. Abdel-Motagly. Review of nonlinear panel flutter at supersonic and hypersonic speeds. *Applied Mechanics Review*, 52:321 – 332, 1999.

[17] HM. Navazi and H. Haddadpour. Parametric study of nonlinear aerothermoelastic behavior of functionally graded plates. *International Journal of Structural Stability and Dynamics*, 9:285 – 293, 2009.

[18] N. Noda. Thermal residual stresses in functionally graded materials. *Journal of Thermal Stresses*, 22:477 – 512, 1999.

[19] T. Prakash and M. Ganapathi. Supersonic flutter characteristics of functionally graded flat panels including thermal effects. *Composite Structures*, 72:10 – 18, 2006.

[20] GN. Praveen and JN. Reddy. Nonlinear transient thermoelastic analysis of functionally graded ceramic-metal metals. *International Journal of Solids and Structures*, 35:4457 – 4476, 1998.

[21] H. Shahverdi, V. Khalafi, and S. Noori. Aerothermoelastic analysis of functionally graded plates using generalized differential quadrature method. *Latin American Journal of Solids and Structures*, 13:796 – 818, 2016.

[22] KJ. Sohn and JH. Kim. Nonlinear thermal flutter of functionally graded panels under a supersonic flow. *Composite Structures*, 88:380 – 387, 2009.

[23] AKL. Srivastava, PK. Datta, and AH. Sheikh. Vibration and dynamic instability of stiffened plates subjected to in-plane harmonic edge loading. *International Journal of Structural Stability and Dynamics*, 2:185 – 195, 2002.

[24] Y. Weiliang and EH. Dowell. Limit cycle oscillation of a fluttering cantilever plate. *AIAA Journal*, 29:1929 – 1936, 1991.

[25] H. Zhao and D. Cao. A study on the aero-elastic flutter of stiffened laminated composite panel in the supersonic flow. *Journal of Sound and Vibration*, 332:4668 – 4679, 2013.